NUREG/CR-1537
EGG-2046
Distribution category: R3

GAP CONDUCTANCE TEST SERIES
FUEL CHARACTERIZATION DATA REPORT

Malati K. Charyulu
Deborah K. Kerwin

Published September 1980

EG&G Idaho, Inc.
Idaho Falls, Idaho 83415

Prepared for the
U.S. Nuclear Regulatory Commission
Washington, D. C. 20555
Under DOE Contract No. DE-AC07-76IDO1570
FIN No. A6041

ABSTRACT

The physical, chemical, mechanical, and metallurgical properties of the UO_2 fuel used in the Power Burst Facility Gap Conductance Test Series are presented. These data were obtained from nondestructive and destructive examinations of representative fuel pellets, performed by EG&G Idaho, Inc., and by Battelle Pacific Northwest Laboratories. These data characterize the initial fuel condition, and are necessary to understand and evaluate fuel rod behavior during irradiation testing in the Gap Conductance Test Series.

SUMMARY

Nondestructive and destructive examinations and tests were performed on representative samples of the UO_2 used in the Gap Conductance Test Series fuel rods. The examination and test results that characterize the fuel materials properties are necessary to understand and evaluate fuel rod behavior during irradiation testing in the Gap Conductance Test Series. The fuel pellets were fabricated from enriched, ceramic grade UO_2 powder containing 10.0 wt% ^{235}U. Impurity levels in the parent fuel lots were measured in equivalent boron cross section (EBC), and ranged from 2.66 to 4.65 EBC. The pellets were sintered to achieve the nominal densities of 92, 95, and 97% of theoretical density (TD) used in the gap conductance tests. Nominal pellet diameters varied between 10.45 and 10.71 mm; the oxygen-to-uranium ratio ranged from 2.0020 to 2.0028, indicating essentially identical fuel composition; and fuel grain sizes in the pellets ranged from 17 to 29 μm. Scanning electron microscope (SEM) examination of a fuel pellet fracture surface was performed. Surface roughness was measured for one pellet of each density and varied from 1.3 to 2.3 μm arithmetic average finish, with an uncertainty of ± 0.1 μm. High-magnification SEM stereo photographs were taken of the pellet surfaces at each location at which surface roughness was measured. Future work will be performed to calibrate the measurements and the photographs to allow surface roughness of irradiated fuel pellets (which cannot be measured directly) to be quantified from SEM photographs. Resintering tests were performed to characterize the densification propensity of the fuel pellets. With very few exceptions, the increase in density after resintering was less than or equal to 1% TD, with an uncertainty of ± 0.5% TD, indicating that the fuel is quite stable to densification. Fuel thermal conductivity values, calculated from thermal diffusivity measurements, are in good agreement with thermal conductivity results determined by other investigators.

CONTENTS

FIGURES

TABLES

GAP CONDUCTANCE TEST SERIES FUEL CHARACTERIZATION DATA REPORT

1. INTRODUCTION

Light water reactor fuel behavior studies are being conducted by the Thermal Fuels Behavior Program of EG&G Idaho, Inc., as part of the Nuclear Regulatory Commission's Water Reactor Safety Research Program.[1] Experimental data are being obtained under normal and postulated accident conditions from a variety of in-reactor and out-of-reactor experiments for assessment of analytical models developed to predict the behavior of light water reactor (LWR) nuclear fuel rods.

Four tests to evaluate gap conductance in LWR design fuel rods have been performed in the Power Burst Facility (PBF) at the Idaho National Engineering Laboratory (INEL). The tests were conducted to evaluate the effects of variations in the design parameters of initial gap width, fuel density, and fill gas composition on the thermal response of LWR fuel rods. Another important purpose of these tests was to evaluate the two experimental methods being employed at the INEL for obtaining gap conductance information from in-reactor tests: (a) the steady state $\int kdT$ method[2] and (b) the thermal oscillator or power oscillation method.[3]

Four tests have been performed in the Gap Conductance Test Series: Tests GC 2-1, GC 2-2, GC 2-3, and PR-1. The tests were performed with boiling water reactor design test rods with variations in the initial diametral gap widths from 0.11 to 0.38 mm (1.0 to 3.6% of the original fuel pellet diameters); fuel nominal theoretical densities of 92, 95, or 97% of theoretical density (TD); and fill gas compositions of helium, xenon, or argon. Table 1 lists the fuel rod design parameters used in the four tests. The data obtained from Tests GC 2-1, GC 2-2, and GC 2-3 have been analyzed, and correlations developed for estimating gap conductance values and effective fuel thermal conductivities for LWR design fuel rods.[3] Test PR-1 was performed in February 1980, and the test results are presently being analyzed and evaluated.

The purpose of this report is to document the pretest characterization data for the fuel used in the Gap Conductance Test Series. Sections 2 through 6 characterize the fuel pellet fabrication, microstructure, surface roughness, densification, and thermal conductivity, respectively.

Table. 1 Gap Conductance Test Series fuel rod parameter variations

Test	Fuel Rod Designations and Design Parameters			
	GC-501	GC-502	GC-503	GC-504
GC 2-1	0.25-mm gap 97% TD[a] Helium	0.11-mm gap 97% TD Helium	0.25-mm gap 95% TD Argon	0.24-mm gap 95% TD Argon
	GC 522-1	GC 522-2	GC 522-3	GC 522-4
GC 2-2	0.25-mm gap 92% TD Xenon	0.13-mm gap 95% TD Argon	0.13-mm gap 95% TD Helium	0.38-mm gap 95% TD Helium
	GC 523-1	GC 523-2	GC 523-3	GC 523-4
GC 2-3	0.12-mm gap 92% TD Helium	0.13-mm gap 95% TD Xenon	0.38-mm gap 97% TD Helium	0.24-mm gap 92% TD Argon

Table. 1 (continued)

Test	Fuel Rod Designations and Design Parameters			
	GC 524-1	GC 524-2	GC 524-3	GC 524-1
PR-1	0.22-mm gap 95% TD Helium	0.22-mm gap 92% TD Helium	0.22-mm gap 97% TD Helium	0.22-mm gap 97% TD Argon

a. 100% of theoretical density (TD) = 10.96 g/cm^3.

2. FUEL PELLET FABRICATION

Fuel pellets for the Gap Conductance Test Series were fabricated from enriched, ceramic grade UO_2 powder containing 10.0 wt% ^{235}U. The powder was prepared by Battelle Pacific Northwest Laboratories from 18% enriched UO_2, supplied by Aerojet Nuclear Company, and depleted UO_3, supplied by Atlantic Richfield Hanford Company.

The starting materials (18% enriched UO_2 and depleted UO_3) were dissolved, solution blended, and converted to UO_2 powder by precipitation of ammonium diuranate (ADU), followed by hydrogen reduction. This process produced 10% enriched ADU in two lots (Lots 3 and 6). The ADU powder lots were then converted to UO_2 powder, maintaining the lot identification, and divided into pellet batches as the pellets were fabricated.

Impurity levels of Lots 3 and 6 were determined by Battelle Pacific Northwest Laboratories before the pellets were fabricated. Table 2 lists the impurity levels in parts per million (ppm) and the equivalent boron cross section (EBC) for Lots 3 and 6. Table 3 presents the uranium content, moisture content, and gaseous impurity levels for the two lots. Total impurity levels were 2.66 and 4.65 EBC, respectively, compared to a specification of 4.00 EBC for the parent fuel material. The variation in EBC between the two lots of fuel was not considered significant.

Fuel pellet fabrication consisted of several steps. The UO_2 powder was first wet-milled and blended, then slugged to a density of ~4 g/cm^3. The slugs were granulated and sieved. An organic lubricant (a wax) was added in various proportions to the finely granulated material, and the material then blended to obtain different densities. (The wax binds the particles together and aids in controlling the final fuel porosity.) The pellets were pressed from this blend to densities between 5 and 6 g/cm^3 and sintered to achieve the desired nominal densities of 92, 95, and 97% of theoretical density (10.96 g/cm^3). The pellets were then ground to specified dimensions. Table 4 lists the impurity levels in ppm and EBC, and Table 5 presents the uranium contents and gaseous impurity levels for all of the fuel batches. Total impurity levels ranged from 3.65 to 6.34 EBC, compared to a specification of 7.00 EBC for the sintered pellets. The following sections characterize the sintering, physical dimensions, and oxygen-to-uranium (O/U) ratio of the fuel pellets.

2.1 Fuel Pellet Sintering

The sintering parameters used were (a) a heating rate of 473 K/h, (b) a constant temperature of 1973 ± 25 K for 8 h, and (c) slow cooling in the furnace. Immersion density measurements of several fuel samples from each batch were performed by Battelle Pacific Northwest Laboratories to determine the sintered densities, and are reported in Table 6.

2.2 Fuel Pellet Dimensions

The nominal pellet dimensions for each Gap Conductance Test Series fuel rod and the corresponding batch and lot numbers are given in Table 7. A centerline hole of ~1.9 mm was drilled in selected pellets after fabrication to accommodate a fuel centerline thermocouple. Individual pellet and thermocouple hole dimensions for the Gap Conductance Tests GC 2-1, GC 2-2, and GC 2-3 fuel pellets are published in References 4, 5, and 6, respectively. Documentation for Test PR-[illegible] is not yet available.

2.3 O/U Ratio

The O/U ratio was measured by Exxon Nuclear Idaho Co., Inc., by controlled potential coulometry[7] with a mercury cathode of 1 M H_2SO_4. The U(VI) was determined using a sample of the fuel dissolved in concentrated H_3PO_4. Total uranium (U_{tot}) was measured by oxidation of U(IV) to U(VI) with excess Ce (IV), enabling the O/U ratio to be calculated as $2 + [U(VI)/U_{tot}]$.

The O/U ratios of three pellets, one of each density, were measured and are given in Table 8. The ratios ranged from 2.0020 to 2.0028, indicating essentially identical oxygen content in the pellets examined.

Table 2. Fuel lot impurity analyses[a]

Element	Specification (ppm)	Lot 3 Amount Present (ppm)	Lot 3 EBC[b]	Lot 6 Amount Present (ppm)	Lot 6 EBC[b]
Al	250	115	0.0115	<50	0.0050
Ba		4	0.0004	1	0.0001
B		0.1	0.1000	0.8	0.8000
Cd		2	0.6208	<0.4	0.1242
Ca		25	0.0050	<25	0.0050
Cs		0.1	0.0003	40	0.1280
Cr	200	25	0.0200	25	0.0400
Co	100	0.7	0.0063	10	0.0900
Cu	250	20	0.0180	<20	0.0180
Dy		0.3	0.0244	<0.5	0.0408
Eu		0.03	0.0124	0.5	0.2062
Gd		0.3	1.3314	<0.5	2.2190
Hf		0.1	0.0008	<1	0.0084
Fe	250	64	0.0448	60	0.0420
Li		0.1	0.0146	<0.1	0.0146
Mn	250	10	0.0340	<10	0.0340
Mo	250	44	0.0176	20	0.0080
Ni	200	100	0.1100	<50	0.0550
P	250	2	0.0002	2	0.0002
Sm		0.1	0.0551	<0.5	0.2757
Si	250	60	0.0060	60	0.0060
Ta	250	0.1	0.0002	0.5	0.0009
Sn	250	10	0.0010	<10	0.0010
Ti	250	20	0.0360	200	0.3600
W	250	0.2	0.0003	1	0.0014
V	250	0.2	0.0003	0.3	0.0042
Zn	250	20	0.0360	40	0.0080
Total (EBC[b])[c]			2.66		4.65

a. Determined per ASTM Specification C753-73.

b. Equivalent boron cross section.

c. Includes C, N, Cl, and F values from Table 3.

Table 3. Fuel lot uranium content, moisture content, and gaseous impurity levels

	Specification	Lot 3[a]	Lot 6[a]
^{235}U (wt%)	10.0 ±0.2	10.02 ±0.05	10.03 ±0.05
U (wt%)	87.8 (mininum)	87.76	87.78
H_2O (ppm)	<4000	1550	1180
C (ppm)	<100	96 (0.0004)	69 (0.0003)
N (ppm)	<200	<10 (<0.0180)	<10 (<0.0180)
Cl (ppm)		10 (0.1330)	<10 (<0.1330)
F (ppm)		<5 (<0.00004)	<5 (<0.00004)
C' +F (ppm)	<350		

a. Values in parentheses for C, N, Cl, and F in each lot are boron equivalents. These values are included in impurity totals given in Table 2.

Table 4. Fuel batch impurity analyses

Element	Specification (ppm)	Batch 15		Batches 15 to 21 (composite)		Batch 22		Batches 23 to 25 (composite)		Batches 26 to 28 (composite)	
		Amount Present (ppm)	EBC[a]	Amount Present (ppm)	EBC[a]	Amount Present (ppm)	EBC[a]	Amount Present (ppm)	EBC[a]	Amount Present (ppm)	EBC[a]
Al	300	200	0.024400	300	0.036600	<50	0.006100	<50	0.006100	<50	0.006100
Ba		6	0.000732	10	0.001220	<0.5	0.000061	0.6	0.000073	2	0.000244
Be		<2	0.000030	<2	0.000030	<2	0.000030	<2	0.000030	<2	0.000030
B	1.5	0.1	0.100000	<2	1.999998	0.3	0.300000	1	0.999999	1	0.999999
Ca	100	40	0.006120	100	0.015300	90	0.013770	80	0.012240	95	0.014535
Cd		<2	0.650194	<2	0.650194	<2	0.650194	<2	0.650194	<2	0.650194
Cr	500	50	0.039950	100	0.079900	60	0.047940	50	0.039950	60	0.047940
Co		0.4	0.003696	8	0.073912	5	0.046195	2	0.018478	6	0.055434
Cu	50	<20	0.017360	<20	0.017360	<20	0.017360	<20	0.017360	<20	0.017360
Hf		<0.5	0.000420	<0.6	0.000504	<0.7	0.000588	<0.6	0.000504	<0.6	0.000504
Fe	400	100	0.067200	270	0.181440	100	0.067200	17	0.114240	300	0.201600
Pb	20	<10	0.000110	<10	0.000110	<10	0.000110	<10	0.000110	<10	0.000110
Mg	50	<10	0.000400	<10	0.000400	<10	0.000400	<10	0.000400	10	0.000400
Mn	10	<10	0.034430	<10	0.034430	<10	0.034430	<10	0.034430	10	0.034430
Mo	150	30	0.012090	30	0.012090	16	0.006448	20	0.008060	50	0.020150
Ni	300	<50	0.056100	60	0.067320	50	0.056100	<50	0.056100	50	0.056100
P		0.7	0.000061	7	0.000609	0.7	0.000061	7	0.000609	20	0.001740
Si	400	60	0.003960	<60	0.003960	<60	0.003960	<60	0.003960	<60	0.003960
Ag	30	<10	0.082360	<10	0.082360	<10	0.082360	<10	0.082360	<10	0.082360

Table 4. (continued)

Element	Specification (ppm)	Batch 15		Batches 15 to 21 (composite)		Batch 22		Batches 23 to 25 (composite)		Batches 26 to 28 (composite)	
		Amount Present (ppm)	EBC[a]	Amount Present (ppm)	EBC[a]	Amount Present (ppm)	EBC[a]	Amount Present (ppm)	EBC[a]	Amount Present (ppm)	EBC[a]
Sn		<10	0.000720	<10	0.000720	<10	0.000720	<10	0.000720	<10	0.000720
W		0.3	0.000449	10	0.014960	1	0.001496	0.4	0.000598	100	0.149600
V	2	<0.1	0.000141	50	0.070300	2	0.002812	10	0.014060	0.5	0.000703
Zn	20	25	0.006025	40	0.009640	50	0.012050	30	0.007230	<20	0.004820
Zr		6	0.000174	200	0.005800	1	0.000029	20	0.000580	7	0.000203
Sm		<0.3	0.157373	0.3	0.157373	<0.4	0.209830	<0.3	0.157373	0.3	0.157373
Eu		0.2	0.086795	0.2	0.086795	0.3	0.130192	<0.2	0.086795		
Gd		<0.5	2.097290	<0.6	2.936206	<0.7	2.936206	<0.5	2.097290	<0.6	2.516748
Dy		<0.5	0.048532	<0.7	0.067945	<0.7	0.067945	<0.6	0.058238	<0.6	0.058238
Total (EBC[a])[b]	7		3.65		6.34		4.85		4.51		5.23

a. Equivalent boron cross section.

b. Includes C, N, Cl, and F values from Table 5.

Table 5. Fuel batch uranium content and gaseous impurity levels

	Specification	Batch 15	Batches 15 to 21 (composite)	Batch 22	Batches 23 to 25 (composite)	Batches 26 to 28 (composite)
^{235}U (wt%)	10.0 ± 0.2	10.01	10.00	10.04	10.06	10.06
U (wt%)	87.6 (minimum)	87.94	87.98	88.23	88.17	88.14
O/U	1.990 to 2.020	2.001	2.001	2.000	2.000	1.999
H (ppm)	3	1.9	0.9	1.5	3.4	1.2
C (ppm)	100	24	13	49	27	25
N (ppm)	75	<10	<10	<10	<10	<10
Cl (ppm)	25	<10	<10	<10	<10	<10
F (ppm)	5	<5	<5	<5	<5	<5
Cl + F (ppm)	25	<15	<15	<15	<15	<15

Table 6. Fuel pellet sintered densities

Batch	Lot	Density (g/cm^3)	Density (% TD)
15	3	10.37	94.6
16	3	10.35	94.4
17	3	10.39	94.8
18	3	10.41	95.0
19	3	10.38	94.7
20	3	10.39	94.8
21A	3	10.38	94.7
21B	3	10.39	94.8
22	6	10.35	94.4
23A	6	10.02	91.4
23B	6	10.02	91.4
24	6	10.03	91.5
25	6	10.02	91.4
26A	6	10.50	95.8
26B	6	10.51	95.9
27	6	10.50	95.8
28	6	10.52	96.0

Table 7. Fuel pellet nominal dimensions[a]

Test	Rod	Nominal Pellet Diameter (mm)	Batch	Lot
	501	10.58	28	6
GC 2-1	502	10.71	27	6
	503	10.58	16	3
	504	10.59	16	3
	522-1	10.58	25	6
GC 2-2	522-2	10.71	19	
	522-3	10.71	19	3
	522-4	10.45	22	6
	523-1	10.71	24	6
GC 2-3	523-2	10.70	19	3
	523-3	10.46	26B	6
	523-4	10.59	25	6
	524-1	10.58	21A	3
PR-1	524-2	10.58	25	6
	524-3	10.58	28	6
	524-4	10.58	28	6

a. The pellets were fabricated as circular cylinders 10.57 mm in length, with the pellet ends flat, not dished.

Table 8. Fuel oxygen-to-uranium ratio

Nominal Pellet Density (% TD)	Batch	Lot	Oxygen-to Uranium Ratio
92	23A	6	2.0020
95	20	3	2.0028
97	26B	6	2.0023

3. FUEL PELLET MICROSTRUCTURE

Fuel pellet microstructure was characterized for one pellet of each density. The pellets were fractured transversely by supporting the ends in a V-block and striking the middle of the pellet. One half of each fractured pellet was mounted for metallographic examination to determine grain size and porosity. The fracture surface of the remaining half of the 95% TD pellet was examined with the scanning electron microscope (SEM) to provide fracture information. Fuel grain size, pore size and distribution, and fractography are discussed in the following sections.

3.1 Fuel Grain Size

Radial distribution of the fuel grain size was determined at EG&G Idaho, Inc. Etched photomicrographs of three pellets, one of each nominal fuel density, are presented in Figures 1, 2 and 3. The grain sizes measured at the center, midradius, and edge of each pellet are given in Table 9.

3.2 Pore Size and Distribution

Radial distribution of the fuel pore sizes was determined at EG&G Idaho, Inc. Unetched photomicrographs of three pellets, one of each nominal fuel density, are presented in Figures 4, 5, and 6. The porosities measured at the center, midradius, and edge of each pellet are given in Table 10. The information in Table 10 includes the number of pores of each size at each location and the percent pore area at each location. The percent pore area is the pore area in a region of fuel examined, divided by the area of the region of fuel examined, multiplied by 100. Histograms illustrating the distribution of percent pore area for each of the three pellets are given in Figure 7.

3.3 Fuel Pellet Fractography

One transverse fracture surface of a 95% TD fuel pellet (Batch 16, Lot 3) was examined using the SEM. Figure 8 shows a photomacrograph of the pellet fracture surface, with an SEM composite across one radius. Figure 9 shows higher magnification SEM photographs at the center, midradius, and edge of the fracture surface. As can be seen in Figure 9, the fracturing was transgranular. Cleavage steps typical of brittle glassy fracture are evident. The porosity is evenly distributed, with larger pores apparent at the grain boundaries. The pores are predominantly circular, indicating that the porosity is in equilibrium, as would be expected for sintered fuel.

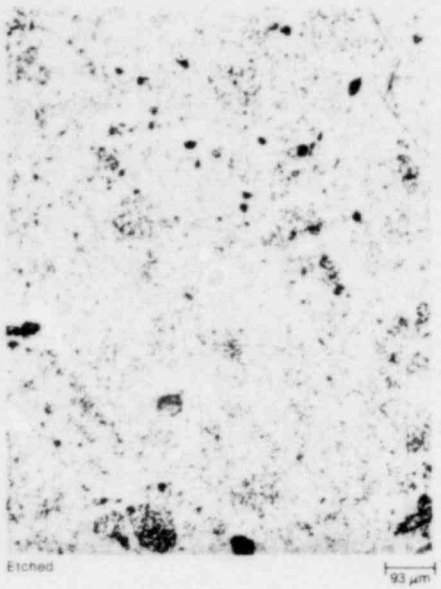

(a) Center

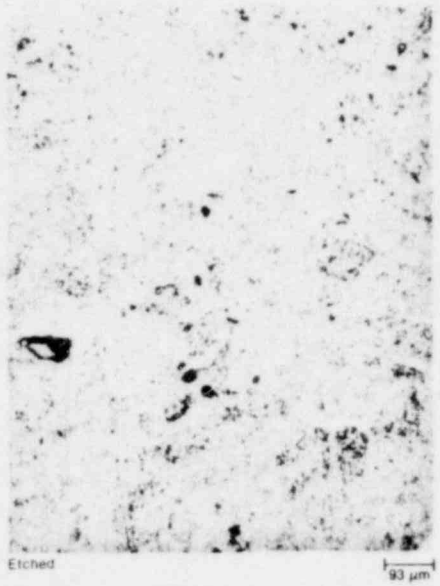

(b) Midradius

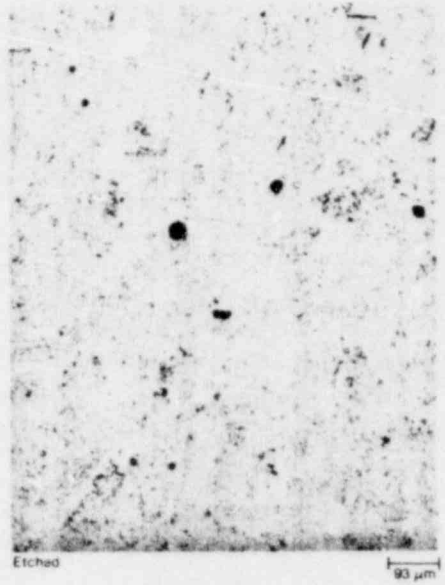

(c) Edge

GS-021-001

Figure 1. Fuel grain size (92% TD fuel).

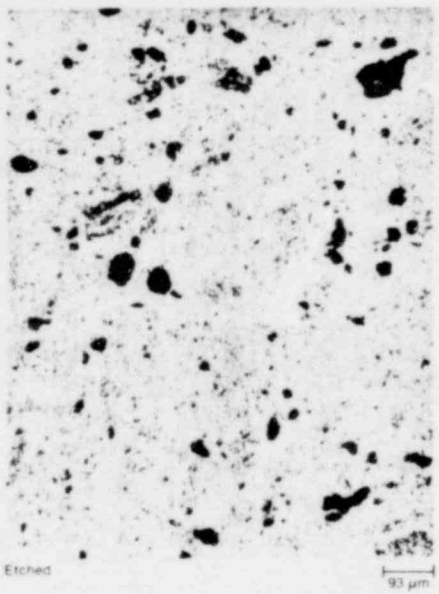

(a) Center

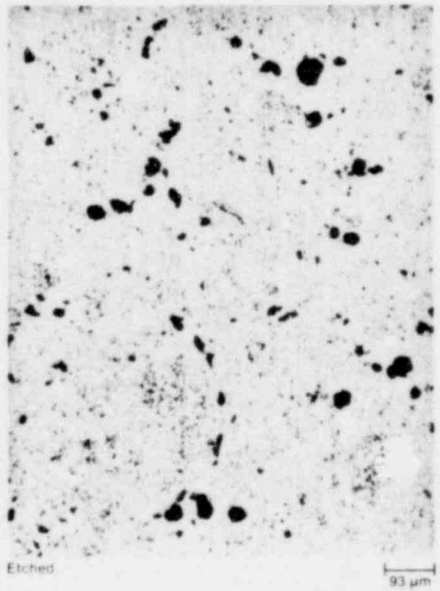

(b) Midradius

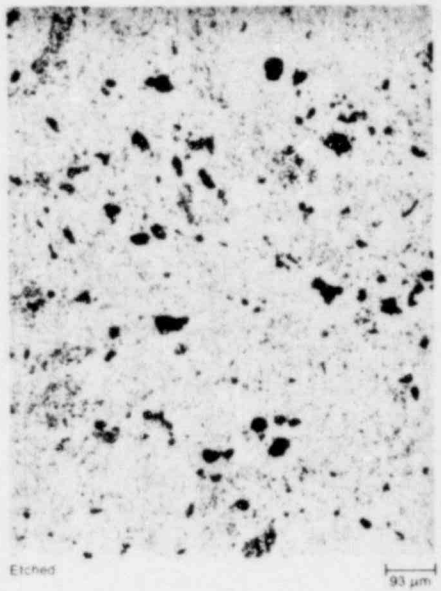

(c) Edge

GS-021-002

Figure 2. Fuel grain size (95% TD fuel).

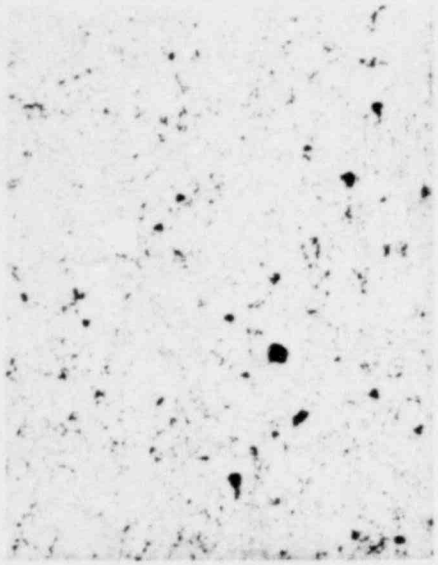

(a) Center

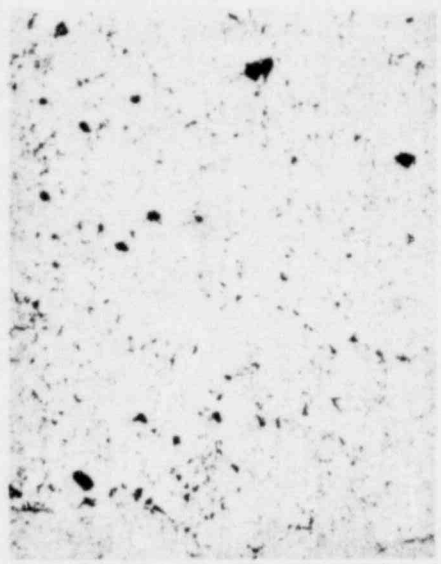

(b) Midradius

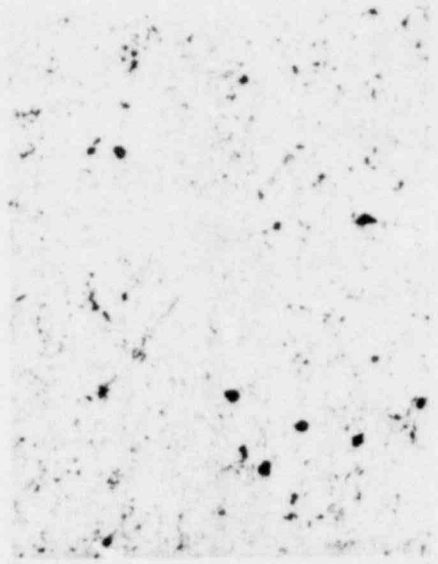

(c) Edge

GS-021-003

Figure 3. Fuel grain size (97% TD fuel).

Table 9. Fuel grain size

Nominal Pellet Density (% TD)	Batch	Lot	Grain Size (μm)		
			Center	Midradius	Edge
92	25	6	20	20	18
95	22	6	22	24	17
97	27	6	29	28	21

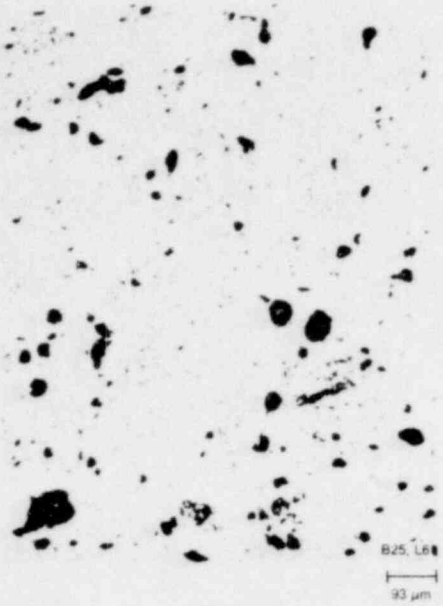

(a) Center

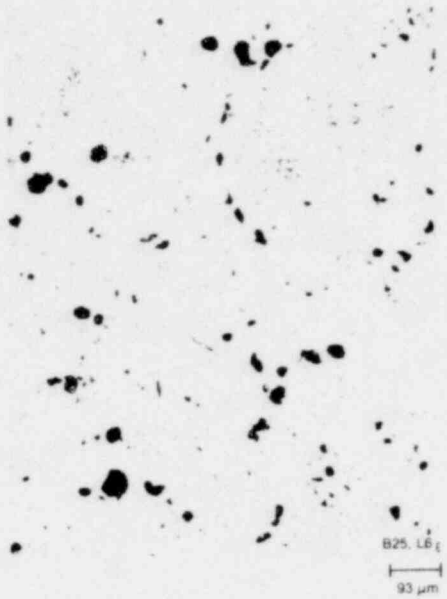

(b) Midradius

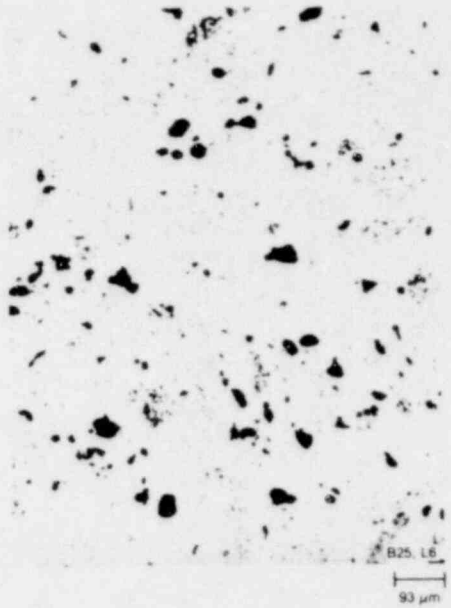

(c) Edge

GS-021-004

Figure 4. Pore size and distribution (92% TD fuel).

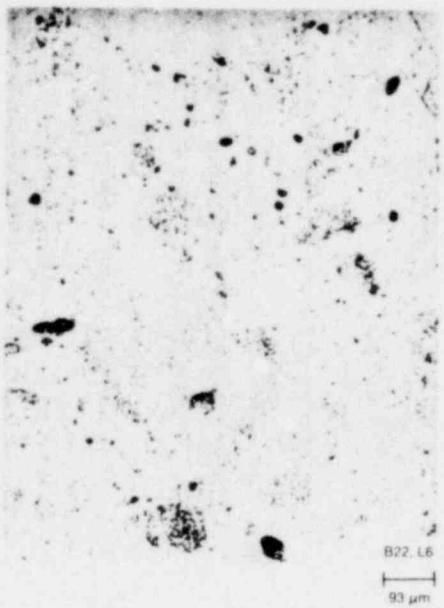

(a) Center

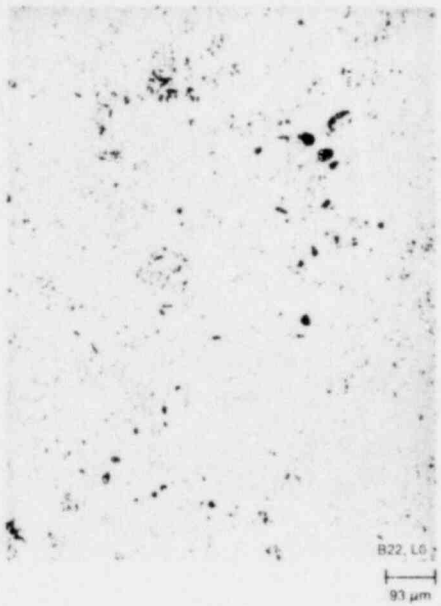

(b) Midradius

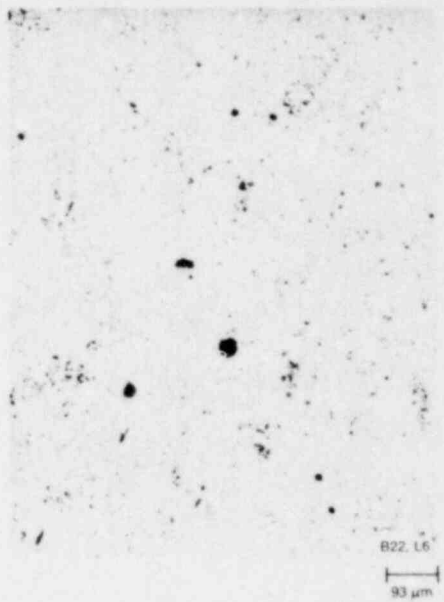

(c) Edge

GS-021-005

Figure 5. Pore size and distribution (95% TD fuel).

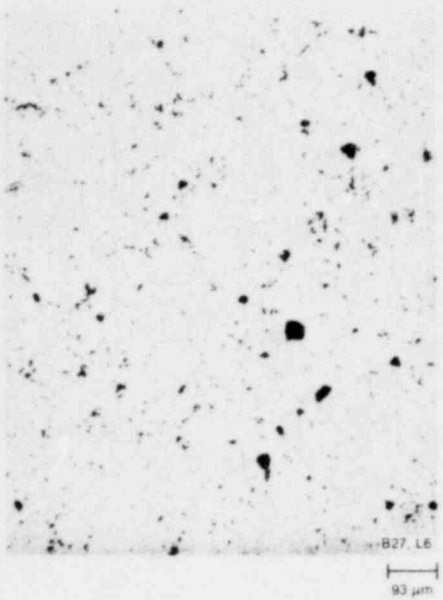

(a) Center

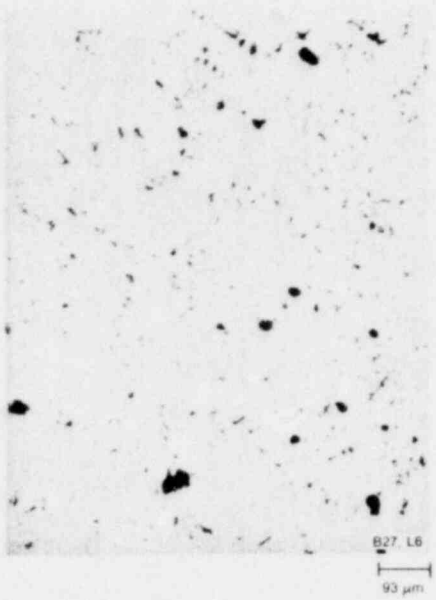

(b) Midradius

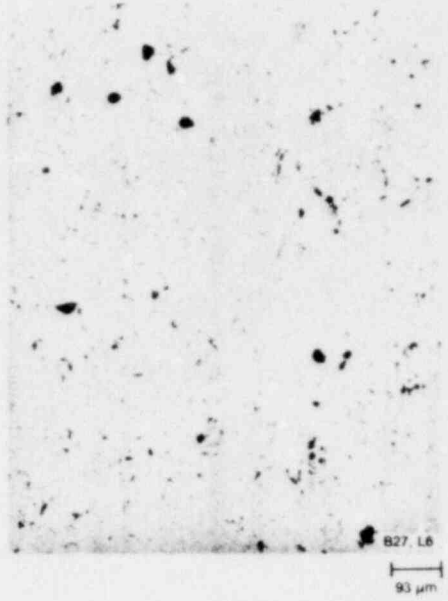

(c) Edge

GS-021-006

Figure 6. Pore size and distribution (97% TD fuel).

Table 10. Fuel pore size and distribution

Pore Diameter (mm)	92% TD Fuel Pellet (number of pores)			95% TD Fuel Pellet (number of pores)			97% TD Fuel Pellet (number of pores)		
	Center	Midradius	Edge	Center	Midradius	Edge	Center	Midradius	Edge
>0.0008	552	602	459	430	378	566	467	450	411
>0.0016	472	520	414	368	336	498	435	380	354
>0.0024	428	462	372	336	307	453	401	339	325
>0.0031	346	365	300	286	259	359	351	302	273
>0.0039	291	290	256	239	232	294	276	259	232
>0.0047	246	237	220	205	191	219	243	218	180
>0.0055	218	201	190	163	158	182	202	165	141
>0.0063	176	158	146	126	129	142	159	131	110
>0.0071	157	137	123	108	117	118	140	117	94
>0.0079	126	114	102	82	92	90	116	93	74
>0.0086	108	95	84	77	77	85	97	82	62
>0.0094	89	83	78	72	65	67	92	74	54
>0.0102	76	77	74	59	61	55	78	62	48
>0.0157	34	38	36	32	33	22	39	31	20
>0.0212	22	23	25	18	14	12	17	14	8
Total pore area (%)	15.7	13.5	15.8	12.7	11.1	10.3	12.2	9.1	7.3

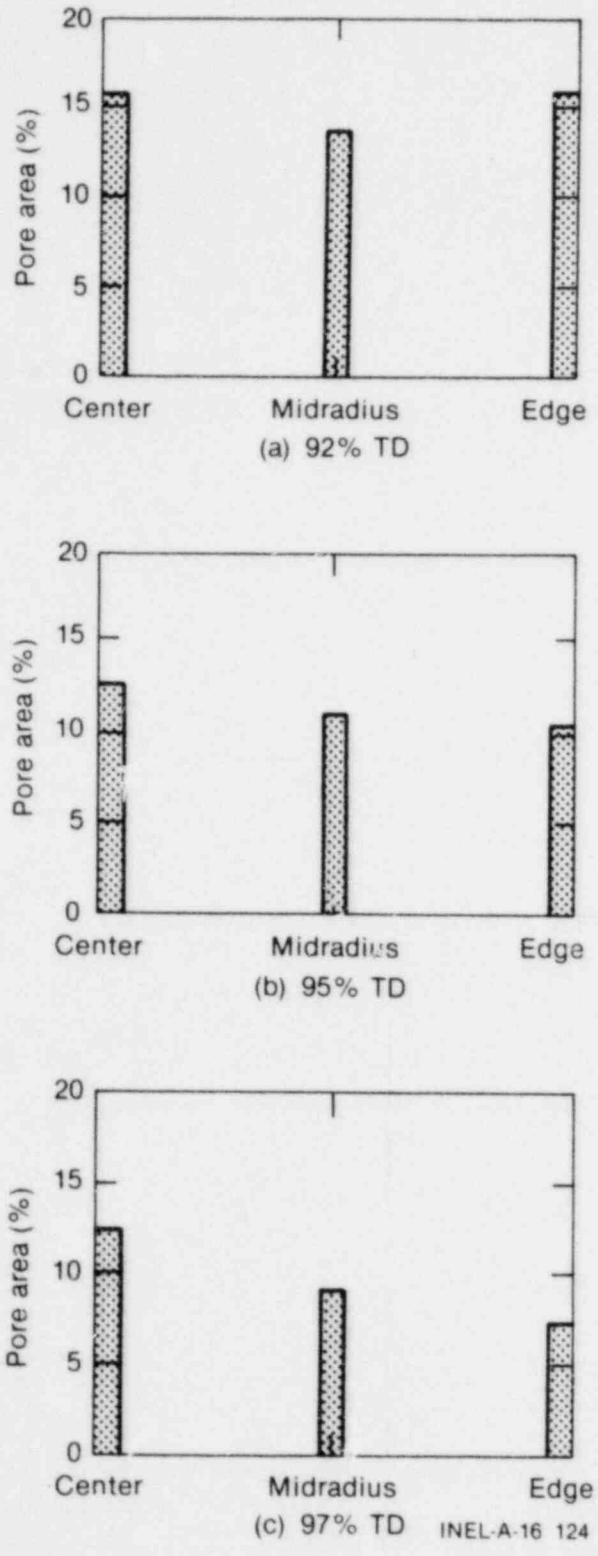

Figure 7. Pore area distributions (92, 95, and 97% TD fuel).

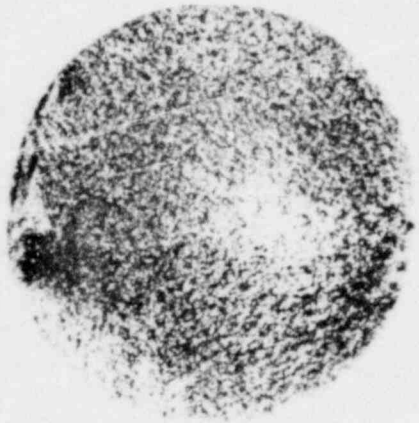

(a) Fuel pellet fracture surface

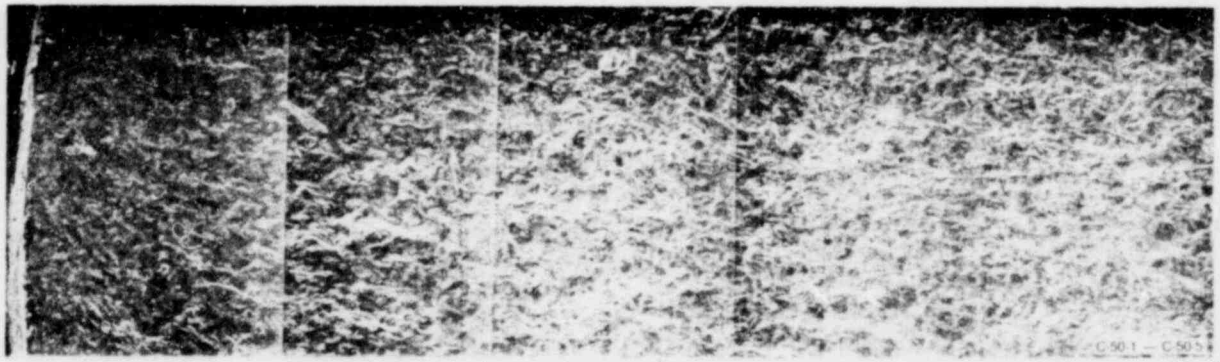

(b) SEM composite of one radius

GS-021-008

Figure 8. Fuel pellet fracture surface from SEM (95% TD fuel).

Figure 9. Fuel pellet fracture surface from SEM at high magnification (95% TD fuel).

4. FUEL PELLET SURFACE ROUGHNESS

Circumferential and axial surface roughness were measured at EG&G Idaho, Inc., for one fuel pellet of each density. Circumferential surface roughness was measured at three axial positions: (a) 1 mm from the top of the fuel pellet, (b) at the axial midplane, and (c) 1 mm from the bottom. Axial surface roughness was measured at four orientations: 0, 90, 180, and 270 degrees. Surface roughness values for all locations ranged from 1.3 to 2.3 μm arithmetic average (AA) finish, with an uncertainty (3σ) of ± 0.1 μm, and are presented in Table 11. Circumferential surface roughness traces for each of the three densities (92, 95, and 97% TD) are shown in Figures 10, 11, and 12, respectively. High-magnification SEM photographs were taken of each fuel pellet (shown in Figures 13, 14, and 15, respectively) at 0 degrees at the three axial positions at which circumferential surface roughness was measured. Circumferential marks from grinding the fuel pellets to the specified dimensions during fabrication, and stylus marks from the axial surface roughness measurements at 0 degrees are evident in the figures. Extensive SEM stereo photography was performed of each fuel pellet at the three axial positions at which circumferential surface roughness was measured, at 0, 90, 180, and 270 degrees. Future work will be performed to calibrate the measurements and the photographs to allow surface roughness of irradiated fuel pellets (which cannot be measured directly) to be quantified from SEM photographs.

Deviation from roundness was also measured at EG&G Idaho, Inc., for one fuel pellet of each density, at the three axial positions at which circumferential surface roughness was measured. A measure of deviation from roundness is the difference in radius between the largest circle that fits completely inside the roundness trace, and the smallest circle that contains the trace. Deviation from roundness values ranged from 17 to 35 μm, with an uncertainty (3σ) of ± 1 μm, and are presented in Table 11. Deviation from roundness traces for each of the three densities are shown in Figures 16, 17, and 18, respectively.

Table 11. Fuel pellet surface roughness and deviation from roundness measurements

Density (% TD)	Batch	Lot	Circumferential Surface Roughness (μm)[a]			Axial Surface Roughness (μm)[a]				Deviation from Roundness (μm)[b]		
			Top	Middle	Bottom	0°	90°	180°	270°	Top	Middle	Bottom
92	24	6	2.0	1.9	2.0	1.5	1.9	1.8	2.3	33	30	31
95	20	3	1.5	1.4	1.5	1.5	1.4	1.5	1.5	30	20	17
97	28	6	1.5	1.7	1.3	1.7	1.5	1.7	1.8	35	30	25

a. The surface roughness values refer to the arithmetic average finish of the pellet surface (Figures 10, 11, 12). Uncertainty (3σ) in this measurement is ± 0.1 μm.

b. The roundness values refer to the difference in radius between the largest circle the fits completely inside the trace (Figures 16, 17, 18) and the smallest circle that contains the trace. Uncertainty (3σ) in this measurement is ± 1 μm.

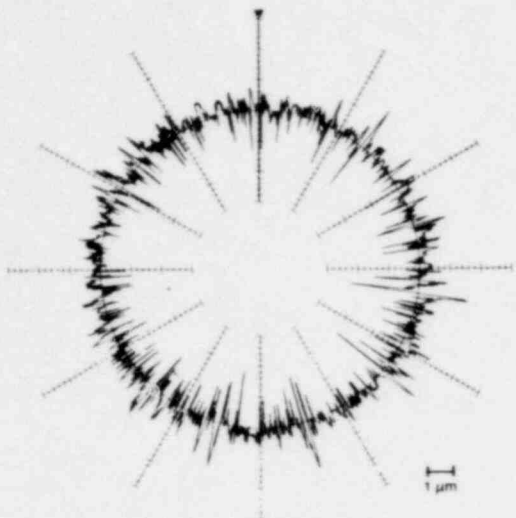

(a) Top of fuel pellet (2.0 μm AA finish)

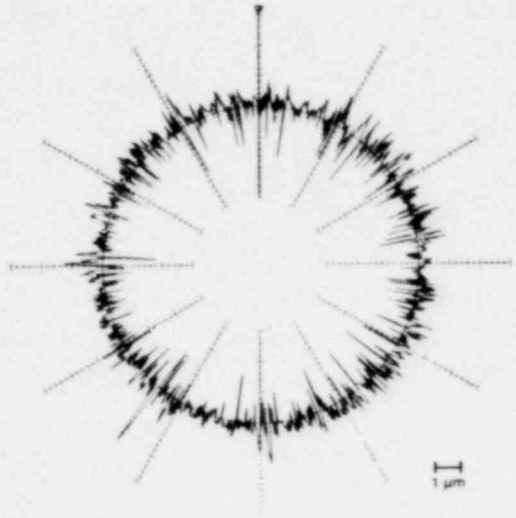

(b) Middle of fuel pellet (1.9 μm AA finish)

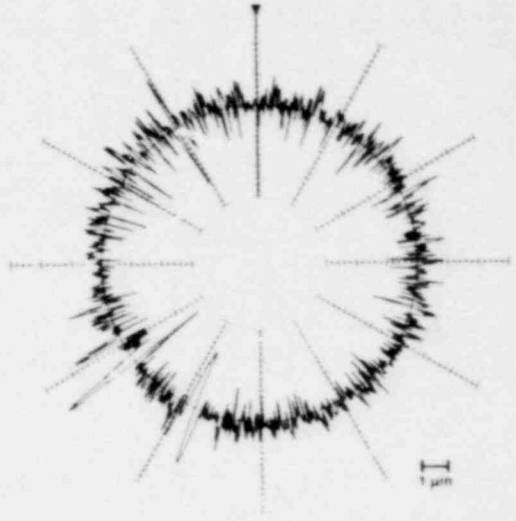

(c) Bottom of fuel pellet (2.0 μm AA finish)

INEL-B-16 128

Figure 10. Surface roughness measurements (92% TD fuel pellet).

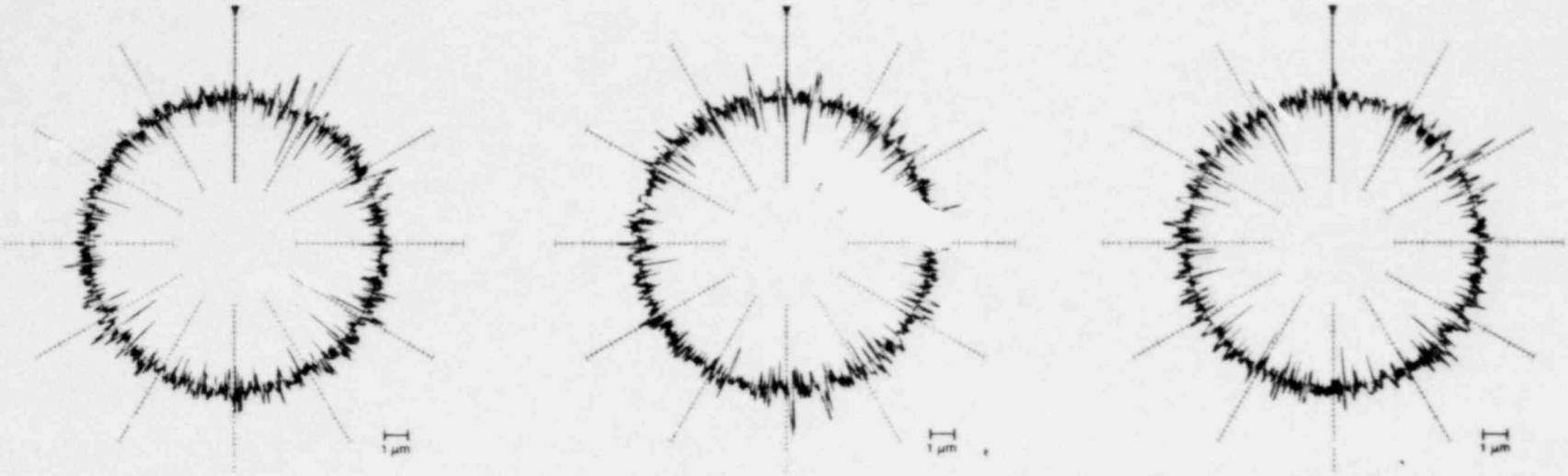

(a) Top of fuel pellet (1.5 μm AA finish)

(b) Middle of fuel pellet (1.4 μm AA finish)

(c) Bottom of fuel pellet (1.5 μm AA finish)

INEL-B-16 127

Figure 11. Surface roughness measurements (95% TD fuel pellet).

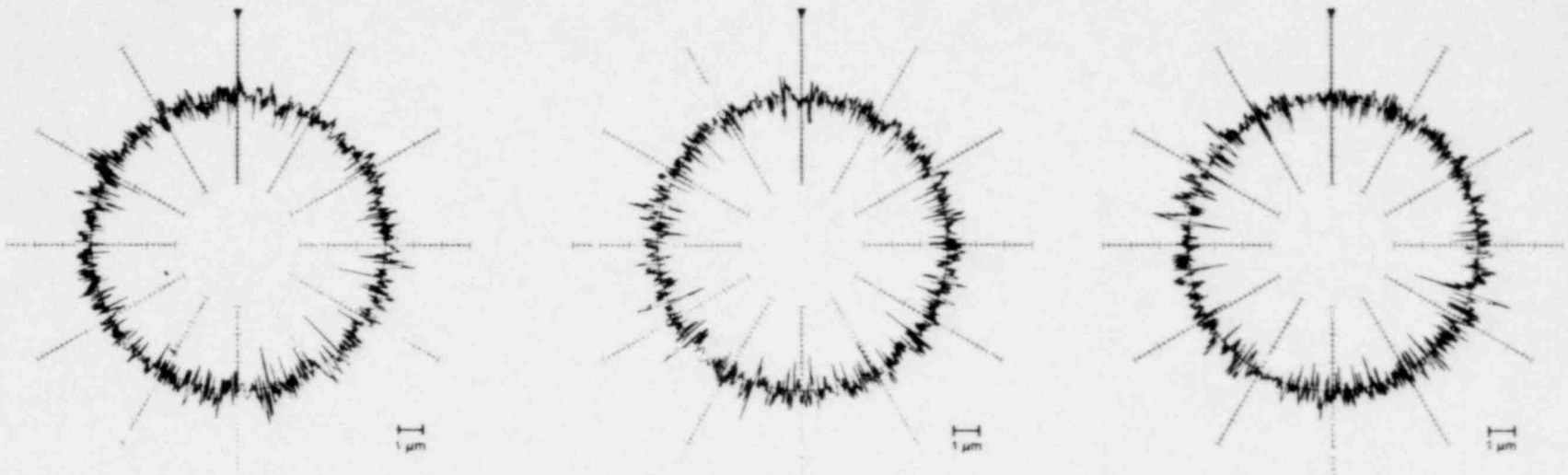

(a) Top of fuel pellet (1.5 μm AA finish)

(b) Middle of fuel pellet (1.7 μm AA finish)

(c) Bottom of fuel pellet (1.3 μm AA finish)

INEL-B-16 130

Figure 12. Surface roughness measurements (97% TD fuel pellet).

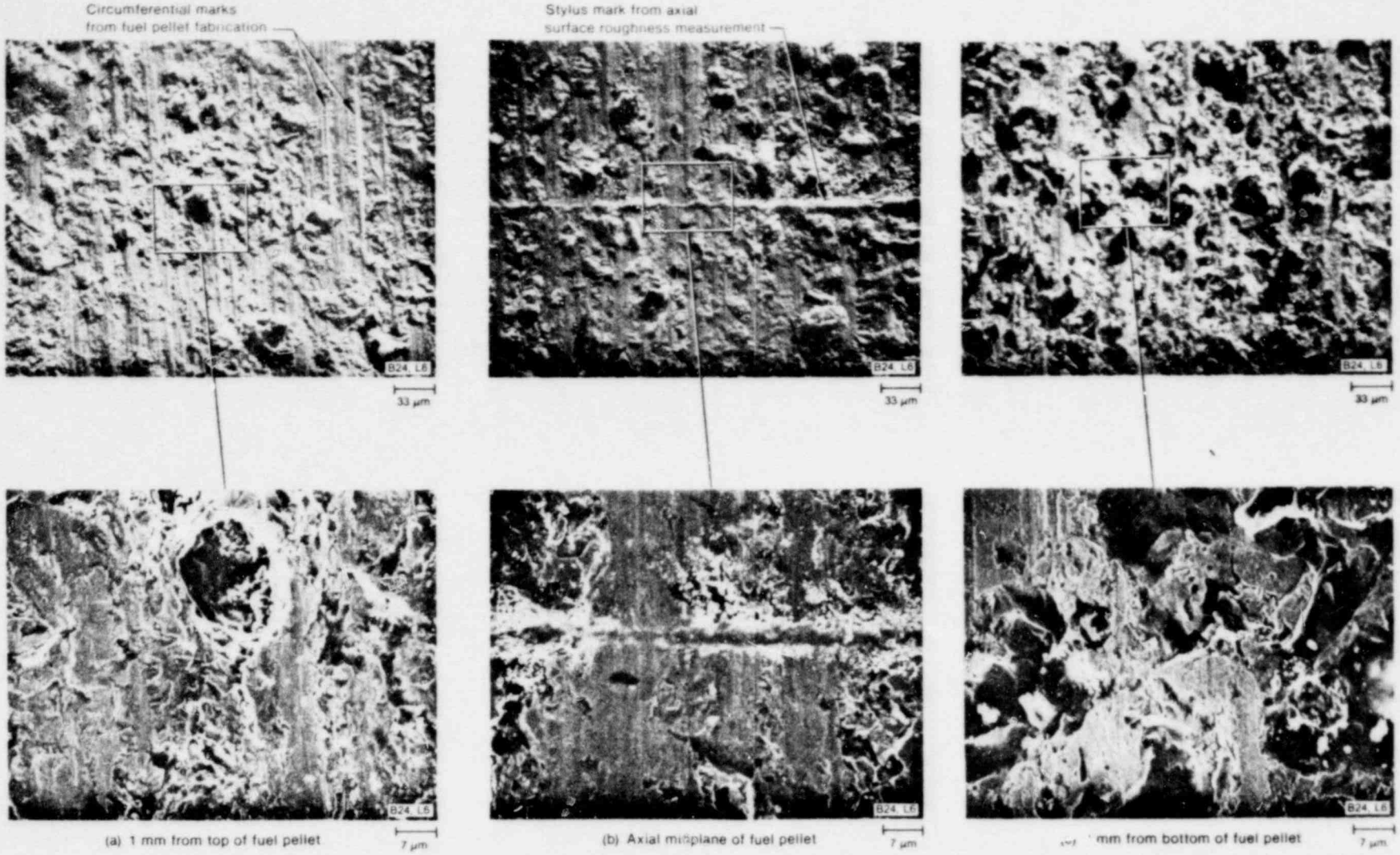

Figure 13. Surface roughness from SEM (92% TD fuel pellet).

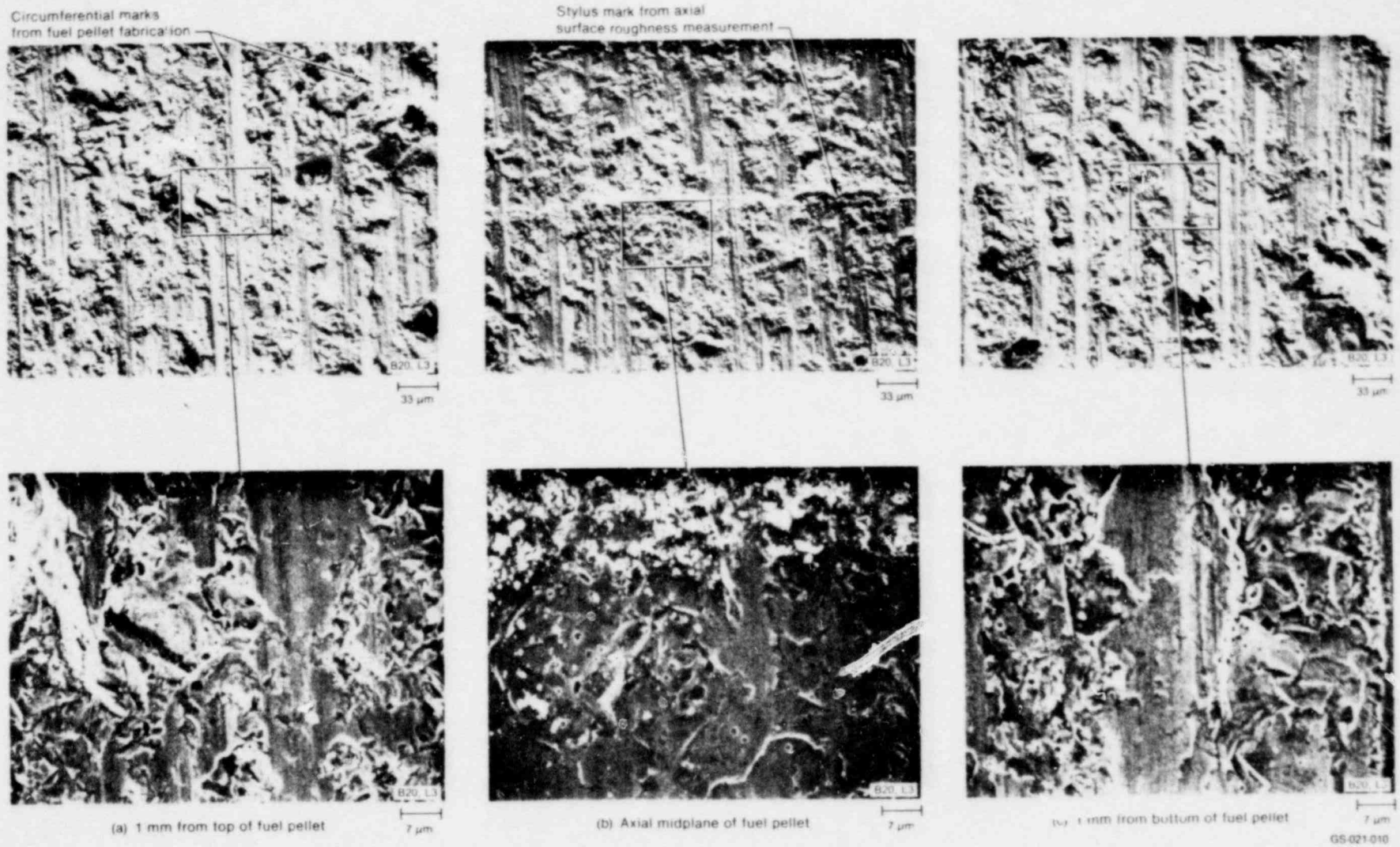

Figure 14. Surface roughness from SEM (95% TD fuel pellet).

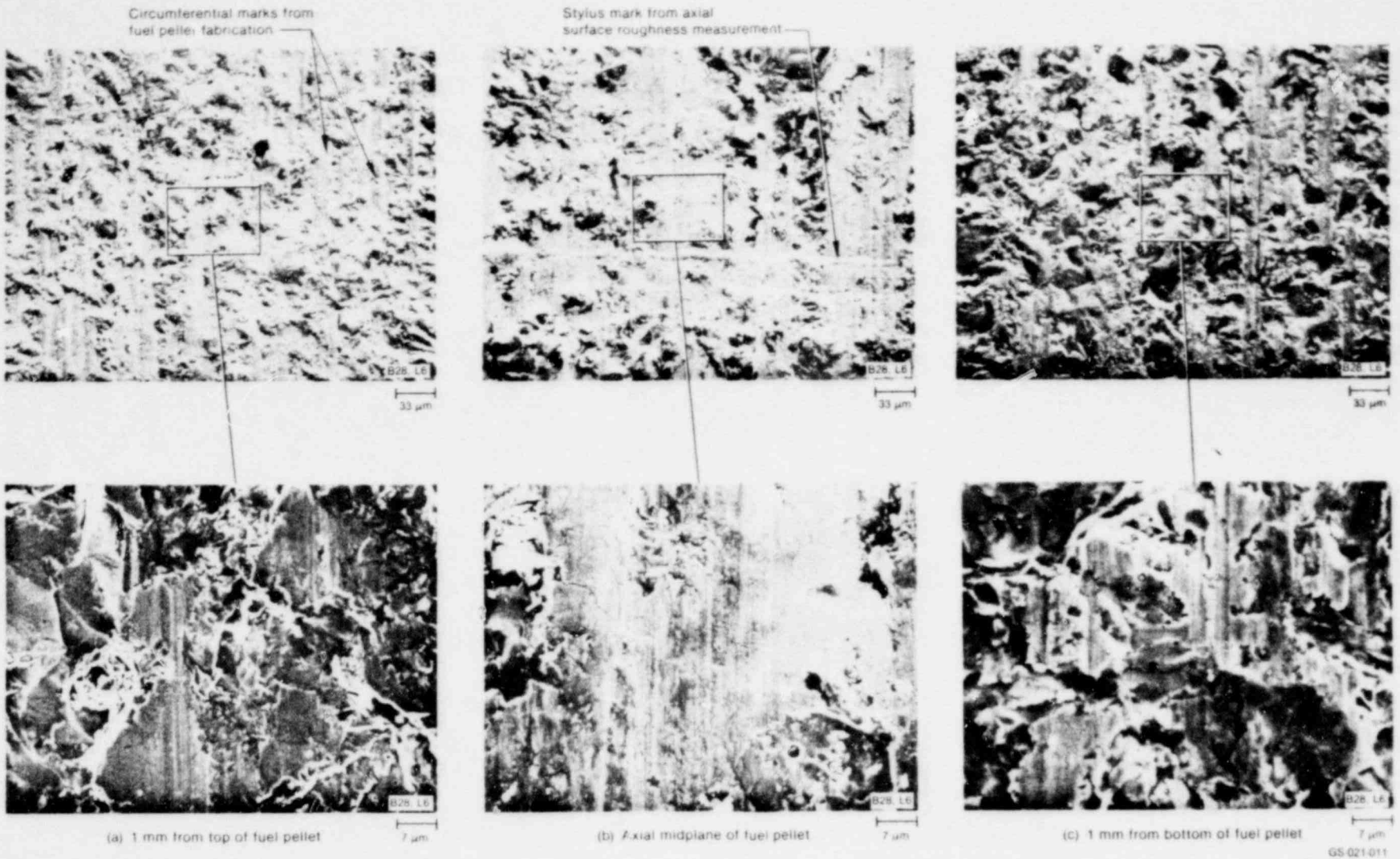

Figure 15. Surface roughness from SEM (97% TD fuel pellet).

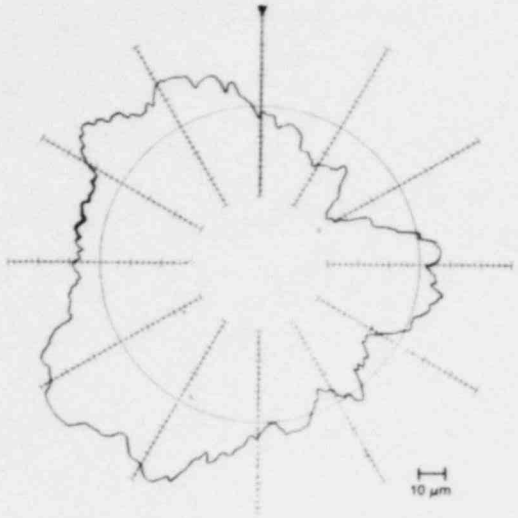

(a) Top of fuel pellet (33 μm)

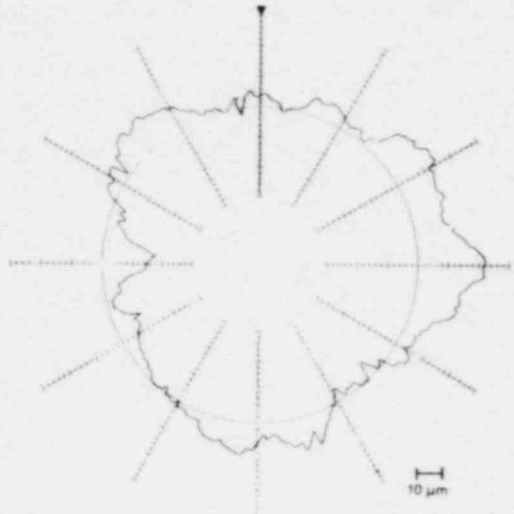

(b) Middle of fuel pellet (30 μm)

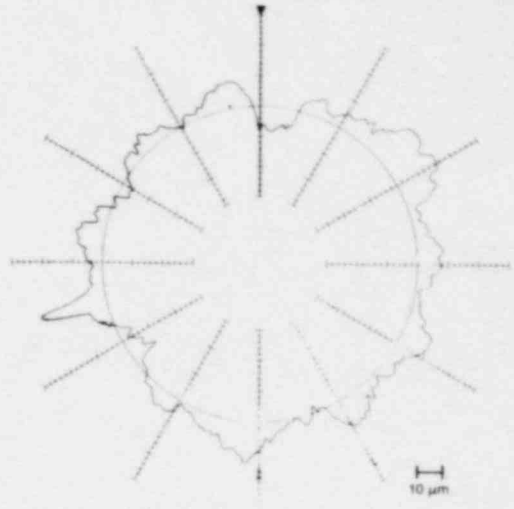

) Bottom of fuel pellet (31 μm)

INEL-B-16 125

Figure 16. De[illegible] roundness measurements (92% TD fuel pellet).

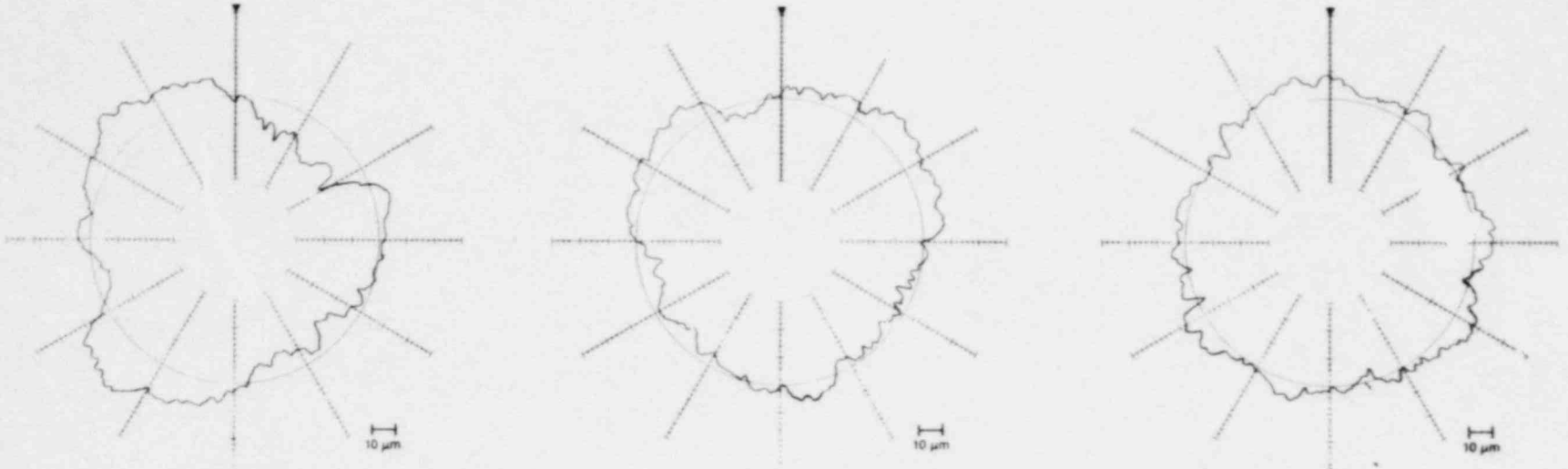

(a) Top of fuel pellet (30 μm)

(b) Middle of fuel pellet (20 μm)

(c) Bottom of fuel pellet (17 μm)

INEL-B-13 126

Figure 17. Deviation from roundness measurements (95% TD fuel pellet).

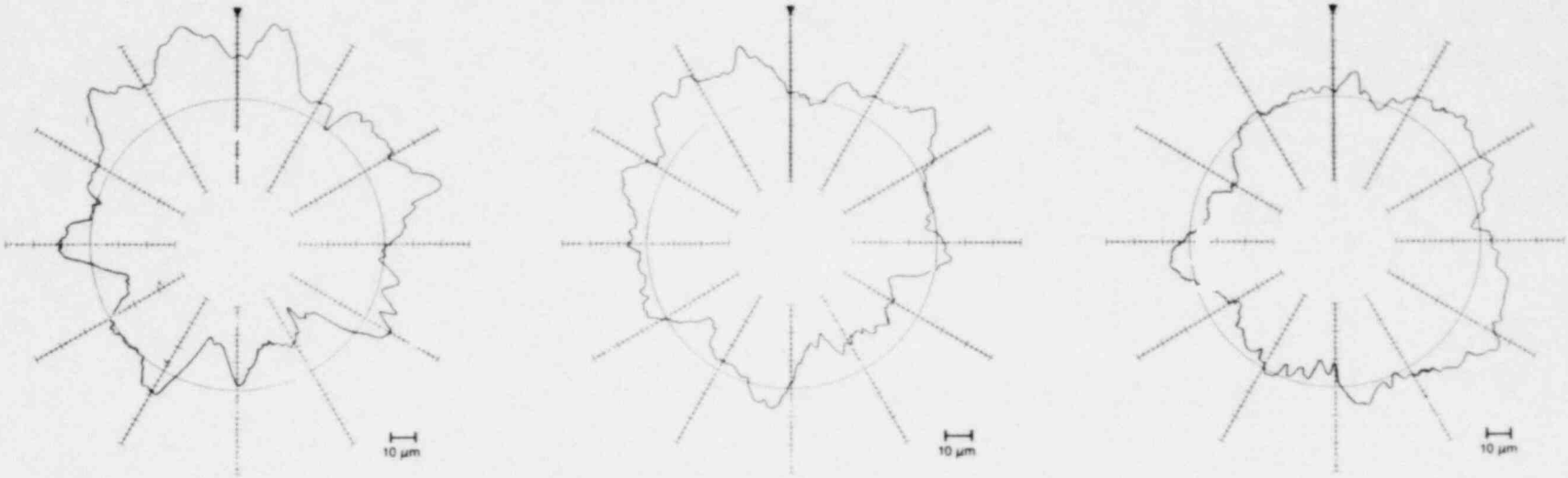

(a) Top of fuel pellet (35 μm)

(b) Middle of fuel pellet (30 μm)

(c) Bottom of fuel pellet (25 μm)

INEL-B 16 129

Figure 18. Deviation from roundness measurements (97% TD fuel pellet).

5. FUEL PELLET DENSIFICATION

Resintering tests were performed at EG&G Idaho, Inc., to characterize the densification propensity of the fuel pellets. Resintering was performed in two groups (with one pellet each from Batches 16, 19, 20, 21A, 21B, 22, 23A, 24, 25, 26A, 27, and 28 in each group) for verification of the measurements. The fuel pellets were resintered by heating at a rate of 473 K/h to 2073 K, holding the temperature constant for 14 h, and cooling at 473 K/h to room temperature. Immersion density measurements were performed before and after resintering using the method described in Reference 8, and the results are presented in Table 12. With very few exceptions, the increase in density after resintering was less than or equal to 1% TD, with an uncertainty (3σ) of ± 0.5% TD. That is, the fuel pellet microstructure is quite stable to densification, and significant in-reactor densification would not be expected.

Table 12. Fuel pellet densification measurements

Group	Batch	Before Resintering[a] (% TD)	After Resintering[a] (% TD)	Increase in Density[a,b] (% TD)
1	16	94.84	95.87	1.03
	19	95.24	95.89	0.65
	20	94.32	95.59	1.27
	21A	95.17	95.74	0.57
	21B	94.57	95.73	1.16
	22	95.32	95.76	0.44
	23A	91.82	92.49	0.67
	24	92.14	92.65	0.51
	25	92.59	93.09	0.50
	26A	96.65	96.92	0.27
	27	95.97	96.33	0.36
	28	96.05	96.88	0.83
2	16	95.59	95.89	0.30
	19	95.41	95.65	0.24
	20	95.42	95.86	0.44
	21A	95.07	94.60	-0.47
	21B	95.44	95.81	0.37
	22	95.09	95.65	0.56
	23A	92.31	92.65	0.34
	24	92.71	93.16	0.45
	25	91.97	92.34	0.37
	26A	96.63	96.79	0.16
	27	95.98	97.49	1.51
	28	96.24	96.99	0.75

a. The uncertainty (3σ) in this value is ± 0.5% TD.

b. After resintering value minus before resintering value.

6. FUEL PELLET THERMAL CONDUCTIVITY

Fuel pellet thermal conductivity was determined over the temperature range of 1070 to approximately 2370 K by Battelle Columbus Laboratories.[9] The flash-laser technique[10,11] for determining thermal diffusivity was employed. Briefly, the method consists of placing a thin, disk-shaped specimen in the isothermal zone of a resistance furnace, and irradiating the specimen with a short-duration pulse from a Nd-doped glass laser. As the heat diffuses through the specimen, the back face temperature rise is measured with an infrared detector. The detector output is displayed on an oscilioscope, and the oscilloscope trace is photographed to provide a permanent record of the back face temperature rise-time relationship. Thermal diffusivity is directly related to this temperature/time relationship.[9] Thermal conductivity values are then calculated from the measured thermal diffusivity values and well-known heat capacity and thermal expansion values as functions of temperature using

$$k = C_p \rho \alpha \quad (1)$$

where

k = thermal conductivity (W/cm·K)

C_p = heat capacity at constant pressure (W·s/g·K)

ρ = density (g/cm^3)

α = thermal diffusivity (cm^2/s).

Thermal diffusivity measurements were performed for two thicknesses of 92% TD fuel and for one thickness each of 95 and 97% TD fuel. For temperatures below 2073 K, each sample was held under vacuum (1.3×10^{-4} Pa). Above 2073 K, the furnace was filled with 6.7×10^4 Pa of argon to reduce UO_2 vaporization. Thermal diffusivity results and calculated thermal conductivity values for the two thicknesses of 92% TD fuel and for the 95 and 97% TD fuel are presented in Tables 13, 14, 15, and 16, respectively. Thermal conductivity values were calculated from Equation (1) using heat capacity values based on the data of Kerrisk and Clifton,[12] and density corrections based on thermal expansion data from Reference 13. Agreement between the data for the two thicknesses of 92% TD fuel is approximately 5% over the entire temperature range, and less than 2% for temperatures above ~1800 K. Figure 19 shows the measured thermal diffusivity values versus temperature for all three densities of fuel. The 92% TD fuel curve was constructed from the data for both thicknesses by linearly interpolating between the data points. Figure 20 presents a comparison of the calculated thermal conductivity values for all three densities of fuel with MATPRO[14] predicted values for 95% TD fuel. The thermal conductivity values for this fuel appear to be in good agreement with the MATPRO predicted values.

Table 13. Measured thermal diffusivity and calculated thermal conductivity values (92% TD fuel pellet[a])

Temperature (K)	Thermal Diffusivity (cm^2/s)	Thermal Conductivity[b] (W/cm·K)
1118	0.00957	0.0300
1203	0.00857	0.0270
12[illegible]	0.00818	0.0260
1428	0.00760	0.0244
1503	0.00726	0.0228
1593	0.00633	0.0206
1693	0.00590	0.0195
1793	0.00585	0.0197
1898	0.00560	0.0194
2008	0.00531	0.0190
2098	0.00517	0.0192
2158	0.00495	0.0188
2278	0.00470	0.0189

a. Batch 24, Lot 6; sample thickness =0.427 mm.

b. Calculated using Equation (1).

Table 14. Measured thermal diffusivity and calculated thermal conductivity values (92% TD fuel pellet, thicker section[a])

Temperature (K)	Thermal Diffusivity (cm^2/s)	Thermal Conductivity[b] (W/cm·K)
1118	0.00918	0.0288
1193	0.00870	0.0274
1303	0.00807	0.0256
1383	0.00784	0.0251
1528	0.00728	0.0235
1548	0.00694	0.0223
1628	0.00677	0.0222
1738	0.00623	0.0208
1828	0.00580	0.0197
1898	0.00564	0.0195
1998	0.00548	0.0196
2088	0.00512	0.0189
2178	0.00507	0.0193
2248	0.00486	0.0192
2348	0.00492	0.0205

a. Batch 24, Lot 6; sample thickness =0.739 mm.

b. Calculated using Equation (1).

Table 15. Measured thermal diffusivity and calculated thermal conductivity values (95% TD fuel pellet[a])

Temperature (K)	Thermal Diffusivity (cm^2/s)	Thermal Conductivity[b] (W/cm·K)
1113	0.01037	0.0338
1243	0.00881	0.0288
1333	0.00816	0.0268
1443	0.00721	0.0239
1533	0.00680	0.0227
1618	0.00663	0.0224
1693	0.00610	0.0209
1793	0.00630	0.0208
1898	0.00578	0.0193
1998	0.00563	0.0183
2098	0.00500	0.0191
2203	0.00477	0.0191
2298	0.00475	0.0200
2348	0.00475	0.0205

a. Batch 19, Lot 3; sample thickness = 0.457 mm.

b. Calculated using Equation (1).

Table 16. Measured thermal diffusivity and calculated thermal conductivity values (97% TD fuel pellet[a])

Temperature (K)	Thermal Diffusivity (cm^2/s)	Thermal Conductivity[b] (W/cm·K)
1073	0.0119	0.0391
1168	0.0108	0.0361
1273	0.0097	0.0324
1373	0.00925	0.0312
1493	0.00772	0.0262
1578	0.00718	0.0247
1673	0.00676	0.0235
1793	0.00625	0.0222
1873	0.00617	0.0224
1993	0.00555	0.0209
2078	0.00544	0.0211
2178	0.00509	0.0206
2278	0.00495	0.0210
2348	0.00495	0.0218

a. Batch 26B, Lot 6; sample thickness = 0.516 mm.

b. Calculated using Equation (1).

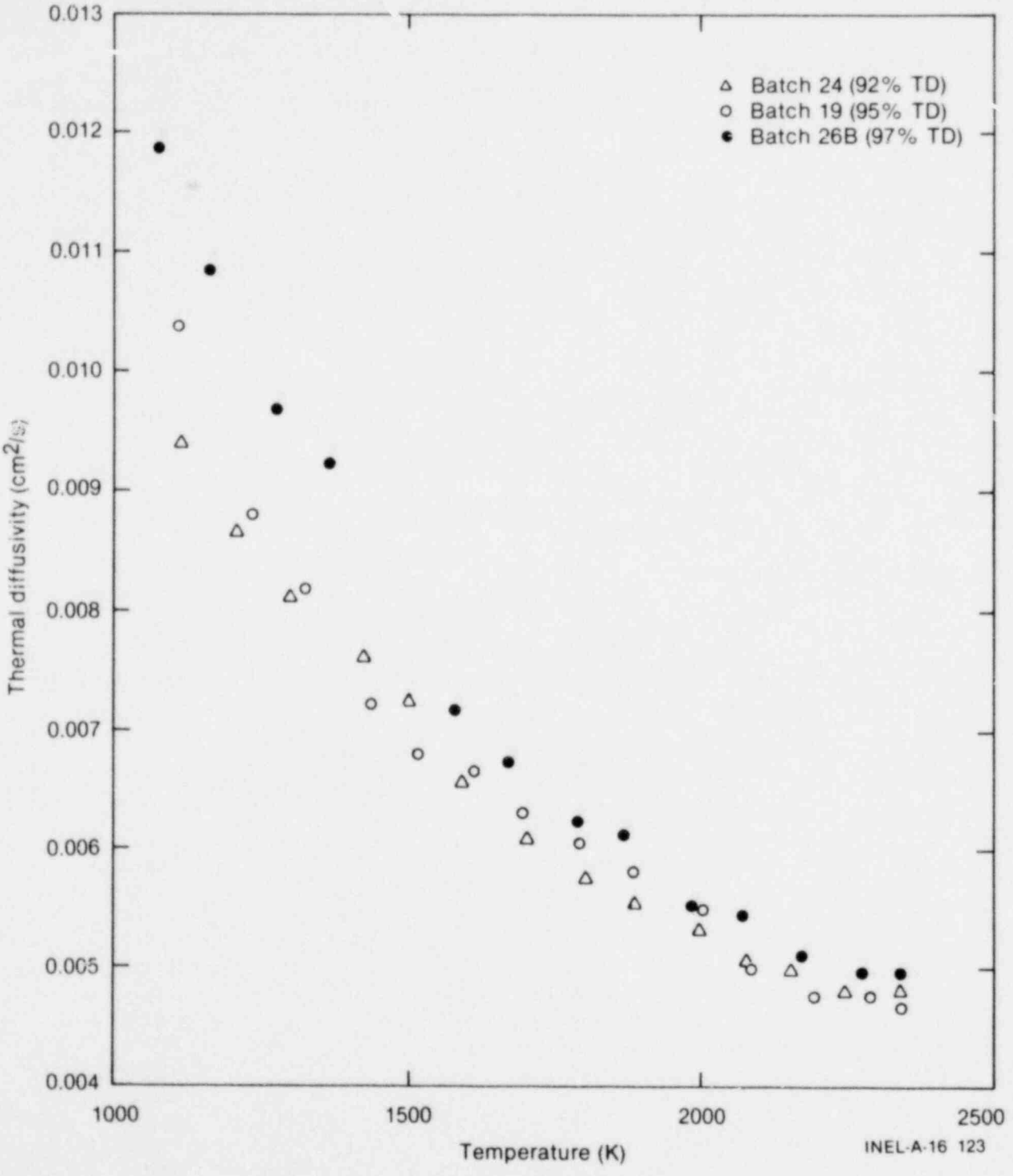

Figure 19. Measured thermal diffusivity values (92, 95, and 97% TD fuel pellets).

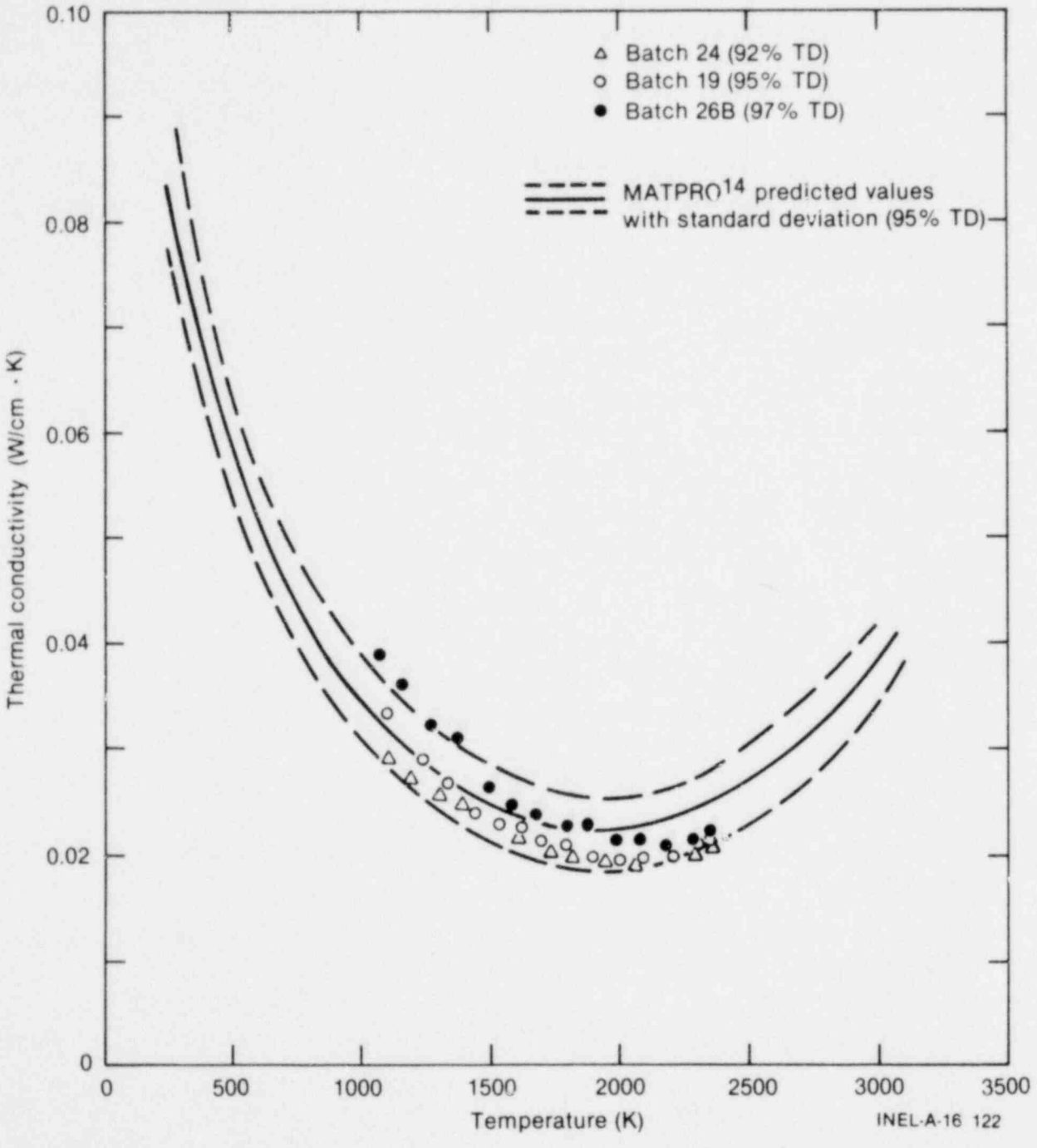

Figure 20. Comparison of calculated thermal conductivity values (92, 95, and 97% TD fuel pellets) with MATPRO[14] predicted values.

7. REFERENCES

1. United States Nuclear Regulatory Commission, *Water Reactor Safety Research Program, A Description of Current and Planned Reactor Safety Research*, NUREG-0006, February 1979.

2. J. A. L. Robertson, *Irradiation Effects in Nuclear Fuels*, New York: Gordon and Breach, Science Publishers, Inc., 1969.

3. R. W. Garner et al., *Gap Conductance Test Series-2, Test Results Report for Tests GC 2-1, GC 2-2, and GC 2-3*, NUREG/CR-0300, TREE 1268, November 1978.

4. B. A. Murdock, *Postirradiation Examination Data Report for Gap Conductance Test Series, Test GC 2-1*, TREE-NUREG-1204, February 1978.

5. D. K. Kerwin, *Postirradiation Examination Data Report for Gap Conductance Test Series, Test GC 2-2*, TREE-NUREG-1206, May 1978.

6. B. A. Cook, *Postirradiation Examination Data Report for Gap Conductance Test Series, Test GC 2-3*, NUREG/CR-0253, TREE-1231, July 1978.

7. J. R. Delmastro, "Research on Analytical Methods," *Technical Quarterly Report, July 1 to September 30, 1978*, ICP-1979.

8. D. K. Kerwin et al., *Power-Cooling-Mismatch Test Series Fuel Rod Material Properties Data Report*, NUREG/CR-0609, TREE-1331, May 1979.

9. M. P. Rausch and C. A. Alexander, *Final Report on Thermal Diffusivity of Uranium Dioxide Fuels of Varying Density to EG&G Idaho*, August 7, 1978, Battelle Columbus Laboratories.

10. C. A. Alexander et al., *Thermal Transport in Plutonium*, BMI-X-688, 1977.

11. M. P. Rausch, *Design of a Flash-Laser Apparatus for Thermal Diffusivity Measurements on Plutonium*, M.S. Thesis, Ohio State University, 1978.

12. J. F. Kerrisk and D. G. Clifton, "Smoothed Values of the Entropy and Heat Capacity of UO_2," *Nuclear Technology, 16*, 1972.

13. P. E. MacDonald and L. B. Thompson, *MATPRO: A Handbook of Materials Properties for Use in the Analysis of Light Water Reactor Fuel Rod Behavior*, ANCR-1263, February 1976.

14. D. L. Hagrman and G. A. Reymann, *MATPRO—Version 10, A Handbook of Material Properties for Use in the Analysis of Light Water Reactor Fuel Rod Behavior*, TREE-NUREG-1180, February 1978.